CFD Simulations of Compressed Air Two Stage Rotary Wankel Expander – Parametric Analysis

Sadiq, Ghada; Tozer, Gavin; Al-Dadah, Raya; Mahmoud, Saad

DOI:
10.1016/j.enconman.2017.03.040

CFD Simulations of Compressed Air Two Stage Rotary Wankel Expander – Parametric Analysis

Ghada A. Sadiq [a, b], Gavin Tozer [a], Raya Al-Dadah [a], Saad Mahmoud [a]

[a] School of Engineering, University of Birmingham, Birmingham, United Kingdom
[b] Al-Mustansiriya University, Baghdad, Iraq
GAS312@bham.ac.uk

ABSTRACT

A small scale volumetric Wankel expander is a powerful device for small-scale power generation in compressed air energy storage (CAES) systems and Organic Rankine cycles powered by different heat sources such as, biomass, low temperature geothermal, solar and waste heat leading to significant reduction in CO2 emissions. Wankel expanders outperform other types of expander due to their ability to produce two power pulses per revolution per chamber additional to higher compactness, lower noise and vibration and lower cost. In this paper, a computational fluid dynamics (CFD) model was developed using ANSYS 16.2 to simulate the flow dynamics for a single and two stage Wankel expanders and to investigate the effect of port configurations, including size and spacing, on the expander's power output and isentropic efficiency. Also, single-stage and two-stage expanders were analysed with different operating conditions. Single-stage 3D CFD results were compared to published work showing close agreement.

The CFD modelling was used to investigate the performance of the rotary device using air as an ideal gas with various port diameters ranging from 15 mm to 50 mm; port spacing varying from 28 mm to 66 mm; different Wankel expander sizes (r = 48, e = 6.6, b = 32) mm and (r = 58, e = 8, b = 40) mm both as single-stage and as two-stage expanders with different configurations and various operating conditions. Results showed that the best Wankel expander design for a single-stage was (r = 48, e = 6.6, b = 32) mm, with the port diameters 20 mm and port spacing equal to 50 mm. Moreover, combining two Wankel expanders horizontally, with a larger one at front, produced 8.52 kW compared with single-stage which gave 4.75 kW power output at the same operating conditions. Also, a maximum isentropic efficiency of 91 % was calculated with inlet pressure of 6 bar and inlet temperature of 400 K at 7500 rpm for the two-stage compared to the 87.25 % for the single-stage.

Keywords: Wankel expander; design consideration; volumetric expansion device; 3D CFD analysis; single and stage-stages.

Nomenclature

b	rotor width (mm)
e	eccentricity (mm)
H	enthalpy (kJ/kg)
k	turbulent kinetic energy (m^2/s^2)
N	shaft speed per second (rpm)
O	origin (-)
p	pressure (N/m^2)
r	rotor radius (mm)
t	time (s)
U	velocity (m/s)
v	volume (m^3)
W	work (J)
x	coordinates in the x direction
y	coordinates in the y direction
Greek symbols	
α	angle (degree)
β	angle (degree)
θ	rotation angle (degree)
φ	velocity angle (degree)
$\boldsymbol{\nu}$	rotor angle (degree)
η	efficiency (%)
ε	dissipation rate (m^2/s^3)
ρ	density (kg/m^3)
μ	viscosity ($N.s/m^2$)
Subscript/superscript	
h	housing
inlet	inlet port
outlet	outlet port
r	rotor
tot	total
Acronyms	
3D	three dimensional
CFD	computational fluid dynamics
UDF	user defined functions
CG	centre of gravity

1. Introduction

Different studies have been carried out since the invention of the rotary engine by Felix Wankel to improve its design and performance [1-3]. Various work reported on the simulation and optimization of the Wankel engine combustion chambers with several fuels such as petrol [4-5], methane and octane [6], hydrogen and diesel [7] and hydrogen enriched ethanol and gasoline [8-9]. Researchers also investigated the effects of apex seals on the performance of the Wankel engine [10-11], whereas others studied the side ports, a micro rotary internal combustion engine [12, 13] and design of the Wankel engine [14]. Wankel engines have also been investigated as part of automotive hybrid systems using electric motor and a Wankel engine as a range extender [15-17]. Furthermore, some studies used the Wankel geometry as a compressor [18-19] and as a pump [20].

Use of a Wankel rotary engine as an expansion device was recently investigated by researchers [21-28]. Badr and coworkers investigated the Wankel expander for power generation using Rankine steam power cycle [21-23]. In [21] they developed a modelling technique and described the performance of the expansion devices for the commercially available Wankel engines of Mazda and Curtiss-Wright for different boiler pressures. While in [22] the design was considered by choosing the geometry; two inlet and two exhaust ports giving two power pulses per revolution. The location of the inlet ports were fixed on the periphery of the rotor housing and the exhaust ports were located on the side housing, in this case the intake system required valves to reach to the optimal design by using a computer-aided-design technique, furthermore material and lubrication for the expansion device were discussed. Their results of (5-20) kW output power was achieved for the Mazda engines (rotor radius 118.5 mm) and the Curtiss- wright engine at 3000 rpm output shaft speed, also the indicated power output and steam mass flow rate of the Mazda Wankel expander were 16.8 kW and 0.12 kg/s respectively, at boiler pressure 6 bar and condenser pressure 1.25 bar. In [23] the performance of Wankel expander was compared with turbines, rotary vane and helical-screw expanders showing the benefits of using the Wankel geometry as an expansion device including compactness, low vibration, low noise and cost. Although both the helical-screw and Wankel expander are the most appropriate devices, some problems remain with using screw expanders, mainly due to the cost of the reduction gear boxes and speed control equipment.

Antonelli et al. [24-27] studied the performance of Wankel expanders with steam and different working fluids for an Organic Rankine Cycle (ORC). Comparison between the numerical modelling software AMESim and experiments in terms of delivered torque, mass flow rate and indicated pressure was carried out in [24] and results were experimentally validated using compressed air. ORC was also used in [25-26]. Their results showed that an expansion isentropic efficiency of around 85 % and thermal ORC cycle efficiency of 10 % were achieved using pentane as working fluid. A small sized power plant using a steam driven Wankel rotary expander and heat generated from renewable sources was investigated theoretically by [27]. Results showed an increase in the thermal efficiency and a noticeable decrease in steam specific consumption up to 25% when comparing the single-stage with multistage Wankel expanders.

The use of the Wankel expander for portable power applications was studied to show the ability of producing electrical power in the order of milliwatts, with an energy density better than batteries [28]. It used a set of intake/exhaust ports to supply the gas from a gas compressor which then expanded in the expander chambers providing a driving pressure to rotate the rotor. In this design the electrical generator was integrated with the rotor to save space and remove the need for an extended crankshaft.

Although Computational Fluid Dynamics (CFD) is powerful tool for detailed three-dimensional simulation and optimization of the developed Wankel engine; there is limited published work regarding the simulation of the Wankel expander. To the authors knowledge the effect on performance of inlet/outlet port configurations, size and spacing has not been considered within the previous literature. Furthermore, there had been no comparison of single-stage with two-stage Wankel expanders. In this study, three-dimensional CFD modelling using ANSYS fluent was developed to investigate different expander configurations with various operating conditions and with compressed air as the working fluid.

2. Wankel expander geometry

The Wankel expander consists of the housing and two moving parts, the rotor and the eccentric output shaft. The rotor’s motion is controlled by two spur gears, an external gear is fixed to the side housing and an internal gear is fixed within the rotor to ensure the rotor tips maintain contact with the housing [29]. The geometry of the rotor housing and flanks are controlled principally by the radius $\boldsymbol{r}$ of the rotor and the eccentricity $\boldsymbol{e}$ of the output shaft. The eccentricity $\boldsymbol{e}$ and the generating rotor radius $\boldsymbol{r}$ are the key dimensions in designing the Wankel rotary expander as shown in Fig. 1.

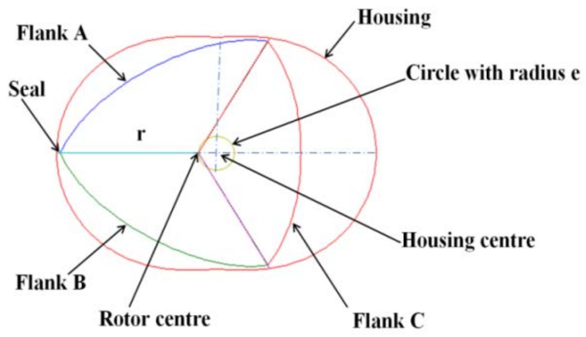

Fig. 1. Definitions of geometric parameters.

The rotor has two simple motions, translation of the rotor centre along the eccentric shaft radius $\boldsymbol{e}$ and rotating around its own centre. The rotor rotates one revolution around its centre whilst the shaft completes three revolutions around the eccentric circle.

The parametric equations of the housing are given as:

$$x_h = e\cos 3\theta + r\cos\theta \tag{1}$$

$$y_h = e\sin 3\theta + r\sin\theta \tag{2}$$

Equations for the rotor shape:

$$x_r = r\cos 2v + \frac{3e^2}{2r}(\cos 8v - \cos 4v) \pm e\left(1 - \frac{9e^2}{r^2}\sin^2 3\,v\right)^{\frac{1}{2}}(\cos 5v + \cos v) \tag{3}$$

$$y_r = r\sin 2v + \frac{3e^2}{2r}(\sin 8v - \sin 4v) \pm e\left(1 - \frac{9e^2}{r^2}\sin^2 3\,v\right)^{\frac{1}{2}}(\cos 5v + \cos v) \tag{4}$$

Where the intervals $\mathbf{v}$ are:

$$\boldsymbol{v} = \left[\frac{\pi}{2}, \frac{5\pi}{6}\right], \left[\frac{11\pi}{6}, \frac{13\pi}{6}\right], \left[\frac{19\pi}{6}, \frac{21\pi}{6}\right]$$

3. Computational fluid dynamic (CFD)

Computational fluid dynamics is very useful for analysing any fluid system effectively before committing to manufacturing. In this case CFD was used to simulate the flow through the Wankel expander, in order to investigate the performance using various port configurations. To achieve this, the software ANSYS Fluent (16.2) was used as it has the capability to allow the mesh to dynamically change with time, which is necessary for the simulation of the complex motion of the Wankel geometry. In order to create the correct movement, user defined functions (UDF's) were written and implemented in Fluent to provide the exact mesh movement at a given rotational speed. The format of UDFs code was developed according to ANSYS Fluent User Guide [30]. The flow chart in Fig. 2 illustrates the major steps used for the CFD simulation work.

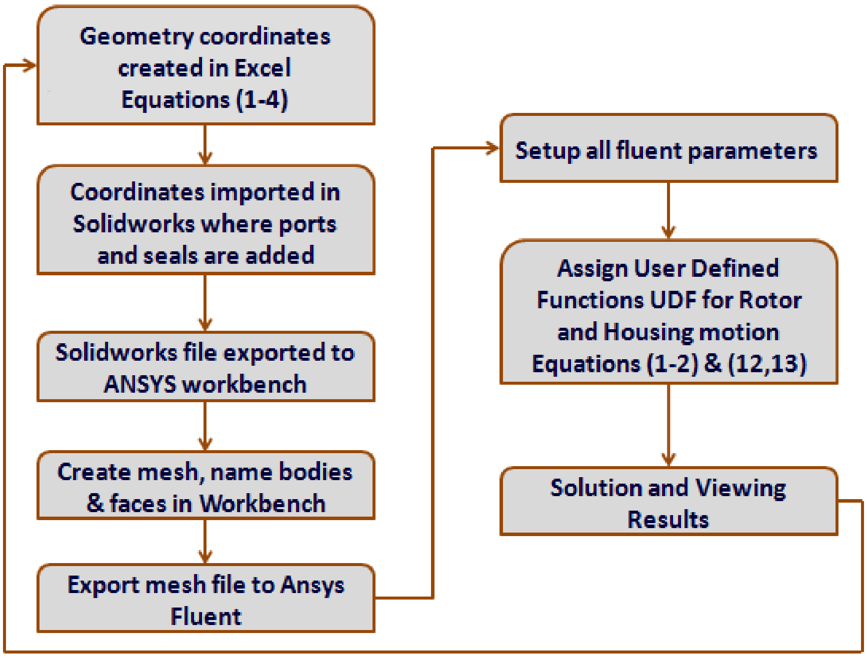

Fig. 2. Flow chart for the CFD modelling steps.

Creation of the rotor and housing geometry was carried out in Solidworks 2015 [31] using an Excel file (2010) [32] with a set of x, y coordinates of both the rotor and housing as detailed in (equations 1-4). These coordinates were then copied into two separate text files (one for the housing and one for the rotor). Once the points were imported as curves in SOLIDWORKS, the shapes could be extruded to create the 3D Wankel geometry. Before the geometry was imported to ANSYS Workbench 16.2, ports and seals were created in order to generate the overall geometry and produce the mesh for the CFD. Tetrahedrons mesh type was used for the 3D Wankel geometry and the effect of mesh size on accuracy (i.e. grid independency) was studied. Grid independency study showed that the solution will be stable and the results not dependent on the number of grid therefore the number of elements of 150000 was used as shown in Fig. 3. While Fig. 4 illustrates the mesh types used in the Wankel expander simulation.

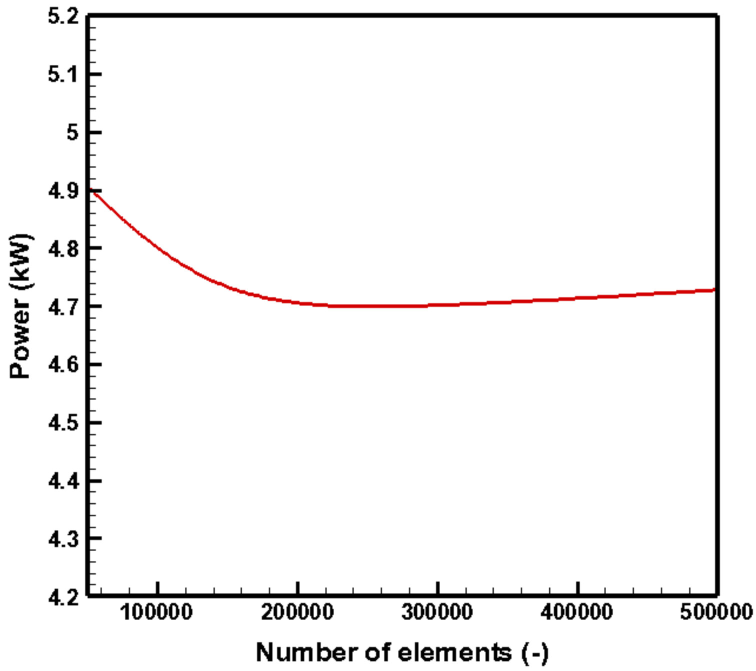

Fig. 3. Effect of mesh density on power output

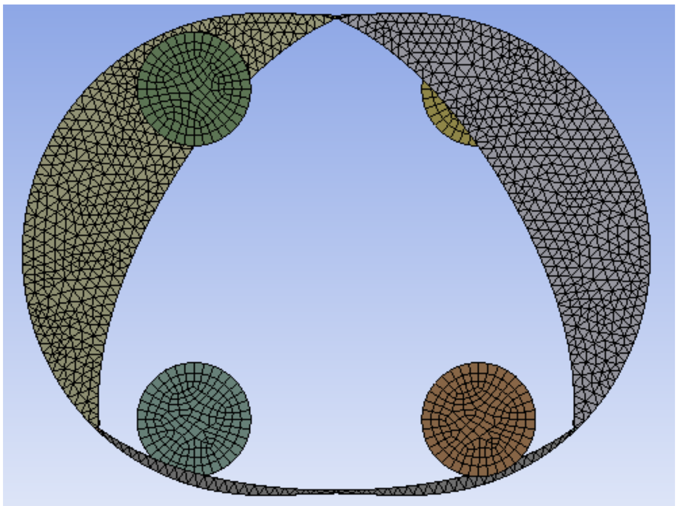

Fig. 4. Wankel expander mesh used

In Fluent solver, some assumptions were considered in the numerical computations as 3D compressible flow, no slip on the wall boundary and adiabatic conditions, atmospheric pressure is 1.013 bar and ambient temperature 300 K as suggested in ANSYS Fluent user guide [30]. The transient solver was selected to allow a time dependant solution, which is important for the Wankel expander simulation through a full cycle (one rotation). Viscous model k-epsilon (RNG) was also required to simulate turbulence and the 'coupled' pressure-velocity coupling scheme was used for 3D simulation. Various boundary conditions as shown in table 2 were input into Fluent representing different operating parameters.

Table 2 The boundary conditions of the Wankel expander

Parameter	Unit	Range/value
Inlet absolute pressure	bar	3-12
Inlet total temperature	K	350- 450
Outlet pressure	bar	1.013
Rotational speed	rpm	1500- 7500

Below are the CFD governing equations which were used for flow modelling, based on conservation of mass, momentum (Navier–Stokes) and energy equations and an equation for modelling the turbulence [33].

Continuity equation:

$$\frac{\partial \rho}{\partial t} + \nabla \cdot \left(\rho \vec{U}\right) = 0 \tag{5}$$

Momentum equation:

$$\frac{\partial (\rho \vec{U})}{\partial t} + \nabla \cdot \left(\rho \vec{U} \times \vec{U}\right) = -\nabla P + \nabla \cdot \vec{\tau} + \overrightarrow{S_M} \tag{6}$$

Energy equation:

$$\frac{\partial (\rho h_{tot})}{\partial t} + \nabla \cdot \left(\rho \vec{U} h_{tot}\right) = -\nabla(\lambda \nabla T) + \mathrm{S_T} \tag{7}$$

where ($\vec{\tau}$) is the stress tensor while S_M and $\mathrm{S_T}$ represent the momentum and temperature source terms respectively.

Turbulence model RNG k-ε equation:

$$\frac{\partial}{\partial t}(\rho k) + \frac{\partial}{\partial x_i}(\rho k u_i) = \frac{\partial}{\partial x_j}\left(\alpha_k \mu_{eff} \frac{\partial k}{\partial x_j}\right) + G_k + G_b - \rho\varepsilon - Y_M + S_k \tag{8}$$

$$\frac{\partial}{\partial t}(\rho \varepsilon) + \frac{\partial}{\partial x_i}(\rho \varepsilon u_i) = \frac{\partial}{\partial x_j}\left(\alpha_k \mu_{eff} \frac{\partial k}{\partial x_j}\right) + C_{1\varepsilon}\frac{\varepsilon}{k}(G_k + C_{3\varepsilon} G_b) - C_{2\varepsilon}\rho\frac{\varepsilon^2}{k} - R_\varepsilon + S_\varepsilon \tag{9}$$

where G_k and G_b symbolize the generation of turbulence kinetic energy. $\mathrm{Y_M}$ describes the turbulence compressibility effects in the k-ε model; S_k and S_ε are user-defined source terms.

User Defined Functions were developed to generate the motion of all volumes in Fluent, using C programming code. The first UDF defined the motion of the rotor where the (DEFINE_CG_MOTION) UDF type was used to give the rotor a constant rotational velocity about its own centre of gravity (CG), whilst translating the centre of gravity with time dependent x and y directional velocity. This results in a circular motion with a radius equal to the eccentricity. The rotation takes three times longer than navigating the eccentric circle.

The Cartesian coordinates of the rotor CG motion:

$$x = e\cos\varphi \tag{10}$$

$$y = e\sin\varphi \tag{11}$$

Where φ = 3θ

Linear velocities of the rotor:

$$\frac{dx}{dt} = -\varphi e\sin\varphi t \tag{12}$$

$$\frac{dy}{dt} = \varphi e\cos\varphi t \tag{13}$$

Issues were encountered when attempting to use the eccentric UDF, mainly negative volume errors. This was due to the speed the apex of the rotor moves past the housing wall, resulting in the apex jumping past more than one node of the housing in a single time step, ultimately allowing cross-over of the mesh faces and producing physically impossible geometry. This could be solved by lowering the time step size, reducing the 'jump' distance of the apex. However, for the model to be accurate, the gap between the rotor apex and the housing wall had to be as small as possible, to minimize leakage between chambers. A smaller gap size resulted in a finer mesh in that area and that in turn meant that the time step has to be even smaller. Consequently, reducing the time step would produce a large increase in simulation run time. Another UDF was created to solve this issue, this time for mesh motion of the housing wall. The UDF translates the nodes of the housing around their periphery mirroring the speed of the rotor apexes. This allows zero relative velocity between the apex and the housing wall, eliminating the primary source of negative volume error; the housing motion is demonstrated in Fig. 5.

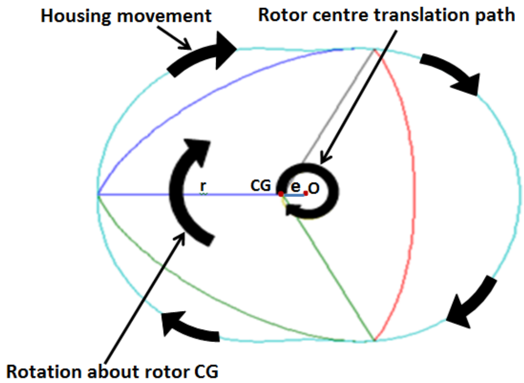

Fig. 5. Housing movement and rotor rotation path

DEFINE_GRID_MOTION UDF type was used as it allows control of individual nodes. The code of the UDF cycles through all nodes of the housing wall and translate each a set distance along the housing geometry, (equations 1-2) for the housing shape were utilised. The following Pseudocode breaks down the steps of the

UDF, the geometric parameters are shown in Fig. 6.

- Retrieve the x and y distance of the selected node from housing centre (O).
- Find beta angle using e, r and (x^2+y^2).
- Find angle alpha.
- Using alpha, determine which quadrant of the housing the node is located in.
- Depending on the quadrant, solve one of the four equations for theta.
- From rotation speed and time step find, find new theta, to match speed of apexes.
- Use new theta with (equations 1-2) to find the new x and y coordinates of the node.
- Repeat steps 1-7 for all nodes on the housing wall.

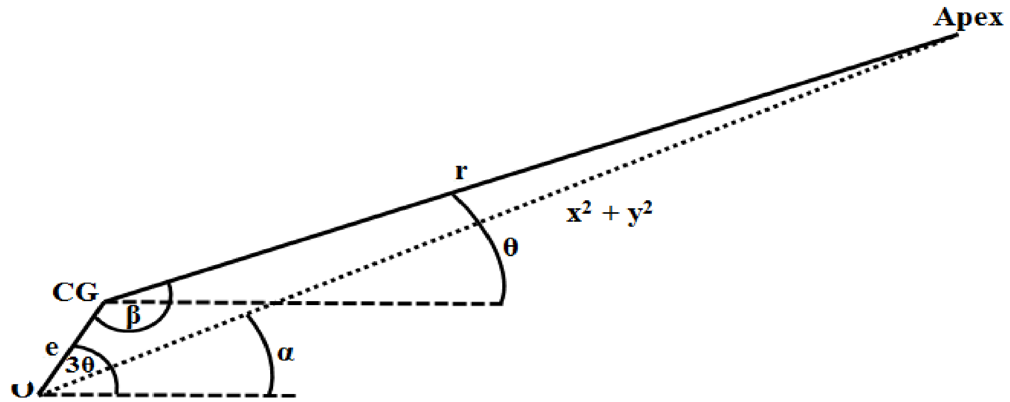

Fig. 6. UDF codes Alpha & Beta & Theta angles

Each run takes around 15 hours (using Intel Core i7-3770 CPU @ 3.40 GHz and 16 GB of RAM). Pressure-Volume (P,V) diagrams were created using the results from ANSYS Fluent allowing the calculation of estimated net work done by each 'chamber' per revolution and this can be converted to power output simply by multiplying it by the output shaft speed (revolutions per second), see (equations 14-15). The following equations were used to calculate the power output. The area enclosed by the pressure-volume curve could be accurately calculated using the trapezoidal function in MATLAB [34] as shown in (equation 16). The isentropic efficiency was calculated using (equation 17).

$$Power\ Output = Work \times Output\ shaft\ speed \tag{14}$$

$$Work = Area\ enclosed\ the\ curve\ (p, v) \tag{15}$$

$$Area\ under\ the\ curve = trapz(p, v) \tag{16}$$

The isentropic efficiency can be calculated by:

$$\eta = \frac{W \times N}{H_{inlet} - H_{outlet}} \tag{17}$$

4. Single-stage expander results

Fig. 7a shows a single-stage Wankle expander where the inlet ports are located on the front side of the expander while the outlet ports were located on the rear side. It is important to identify the location and size for the inlet and outlet ports of the expander to allow the inlet port to open on achieving minimum volume (maximum pressure) and the outlet port should open upon reaching the maximum volume of the chamber [22]. Fig. 7b shows the three dimensional mesh distributions.

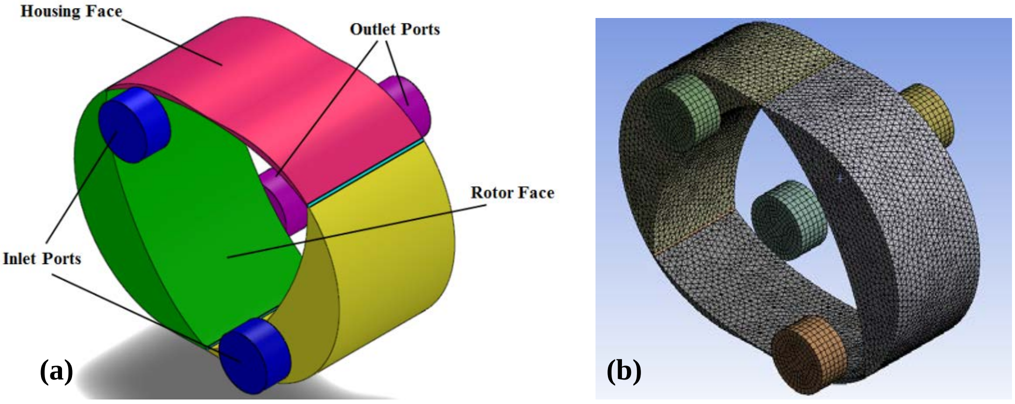

Fig. 7. Wankel Expander geometry (a) and meshes generation (b).

Fig. 8a compares the CFD predicted expander volume at various rotor angles to that reported by [22] using the Mazda Wankel engine with (r = 118.5, e = 17, b = 69) mm showing good agreement. Fig. 8b compares the predicted power output from [22] and the CFD simulation, which are 16.8kW and 17.8kW respectively with a difference of about 6%.

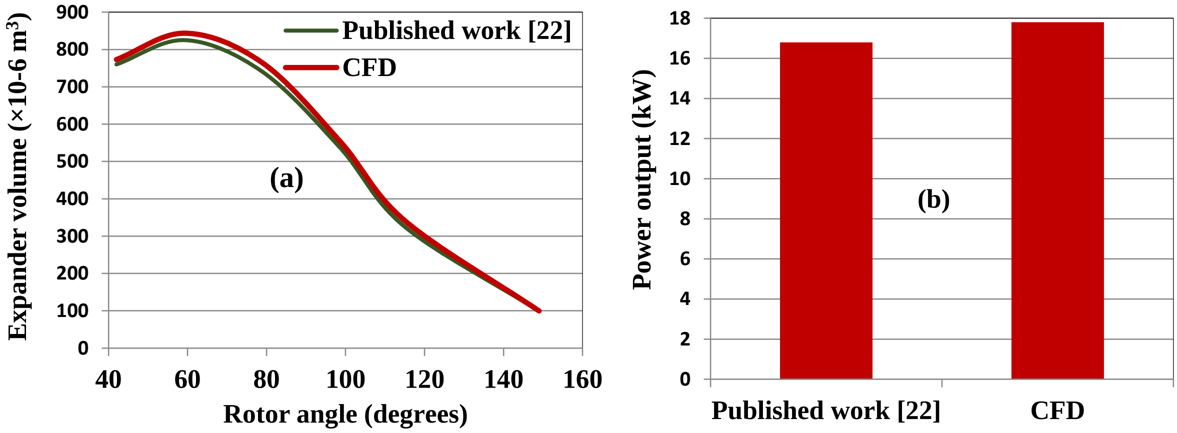

Fig. 8a. Comparison between CFD and published paper [22] results for volume of expander against rotor angle **8b.** Comparison of the power output between CFD and published paper [22].

Fig. 9a,b,c shows the contours of absolute pressure, temperature and velocity vectors for (r = 48, e = 6.6, b = 32) mm and ports diameter 15 mm at inlet pressure equal to 3 bar, inlet temperature 400 K and the output shaft speed of 7500 rpm. These contours and vectors can be viewed for any rotation angle and can therefore be used to ensure the model is behaving as expected.

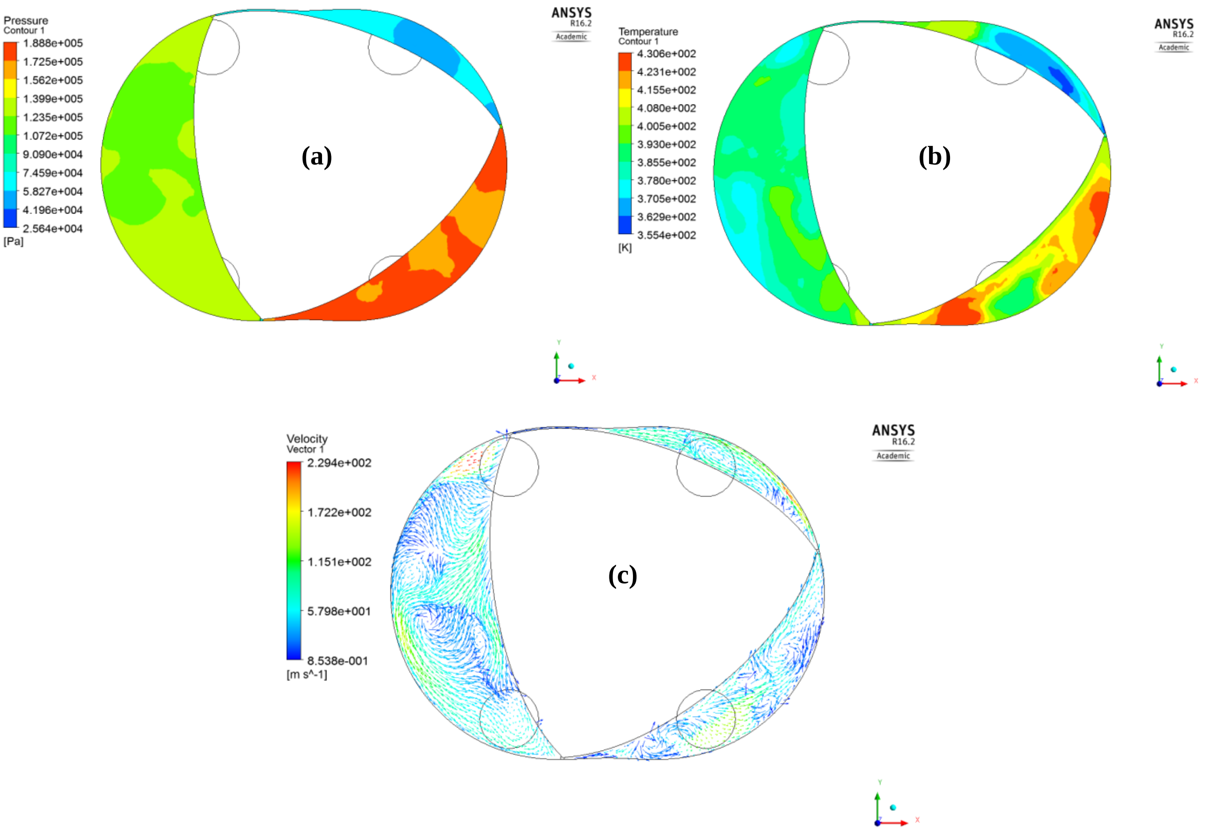

Fig. 9. Contours of absolute pressure (a), temperature(b) and velocity vector (c).

Different port configurations, sizes and locations were simulated, ports diameters (15, 18, 22, 30, 40 and 50) mm, port spacing (28, 44, 57 and 66) mm and various inlet pressures ranging from 3 bars to 6 bars. The port configurations investigated are shown in Fig. 10.

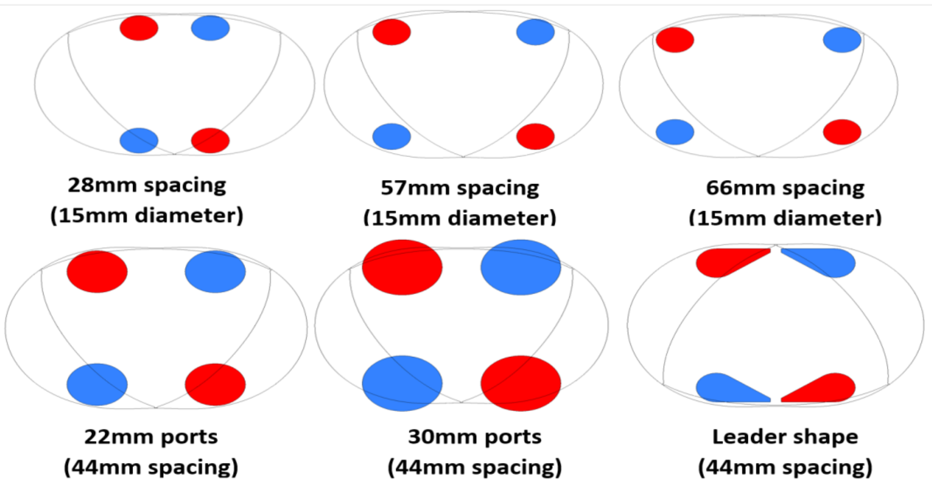

Fig. 10. Ports size, shapes and location configurations.
(Red ports are inlets, blue ports are outlets**)**

Fig. 11 shows the power output at different port diameter and spacing. It can be seen that the peak power output occurs for the diameter size somewhere between 30mm and 40mm and the optimal port spacing for the output shaft speed of 7500rpm is between 44mm and 57mm. However this size is very large and parts of the ports move over the edge of the housing boundary. This could cause other problems in a real expander's operation. Therefore, to optimise power, it would be practical to design the largest possible diameter port without crossing the housing wall boundary.

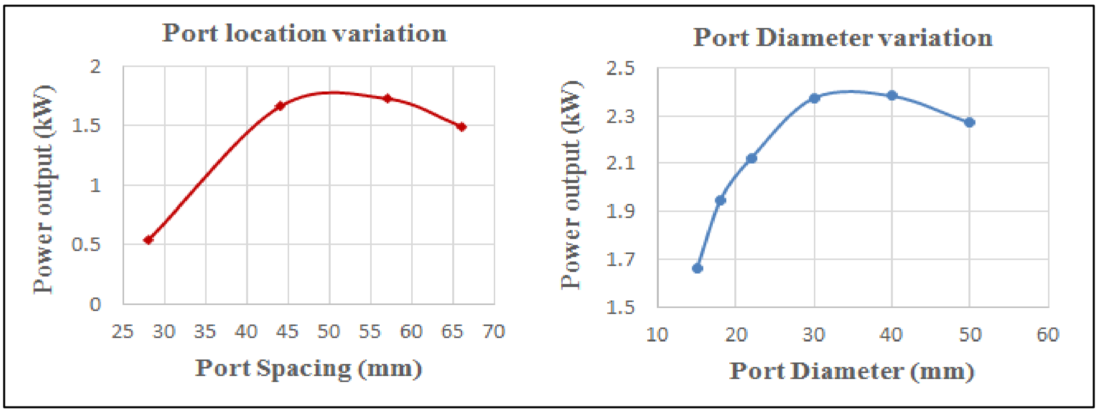

Fig. 11. Power output with increasing port diameter and spacing

The results in Fig. 12 show the power output for the geometry dimensions (e = 6.6mm, r = 48mm, b =32 mm) and operating parameters of inlet pressure 3 bar, inlet temperature 400 K and output shaft speed (7500 rpm). It can be observed that the 'leader' shape ports in the wider positions produce the largest power output. The 8 port configuration is 4 ports on either side of the housing.

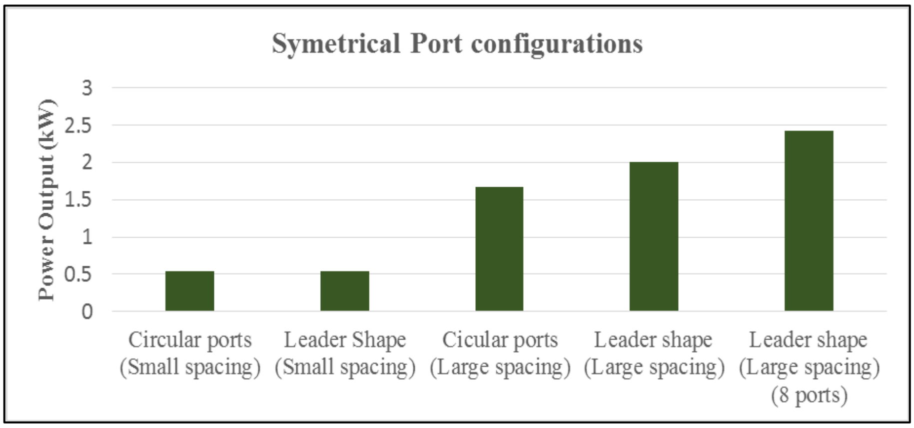

Fig. 12. Power output with different port shapes.

CFD results showed that increasing the spacing between the ports leads to increasing the power output to reach a maximum of 1.8 kW at spacing of 50 mm. As for port diameter, increasing the port diameter will increase the power output to reach a maximum of 2.5 kW at port diameter of 30 mm. However the 20 mm port diameter with 2 kW power output would be the largest practical size for this geometry.

The effect of expander thickness has been investigated for the cases with the rotor radius 48 mm and eccentricity 6.6 mm of (32, 48 & 64) mm. Fig. 13 reports the power output for the three cases and shows that the best power output can be achieved with the thickness of (32) mm.

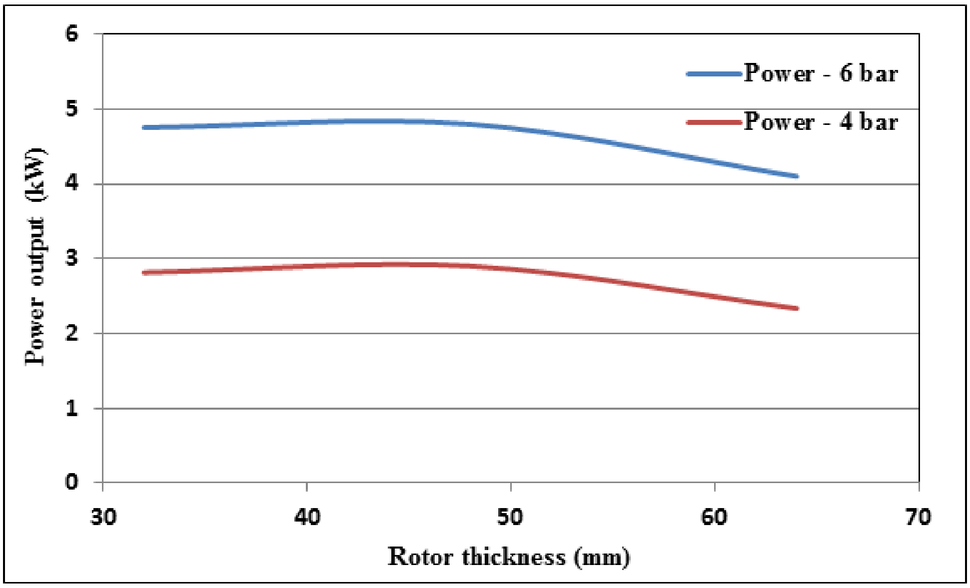

Fig. 13. Power output and an isentropic efficiency of the Wankel expander for different rotor thickness

Fig. 14 shows the CFD predicted power output using the three single-stage Wankel expanders with different dimensions at inlet pressure 6 bar, inlet temperature 400 K and 7500 rpm output shaft speed. It is clear that the best power output achieved was for single-stage (f) reaching 4.75 kW.

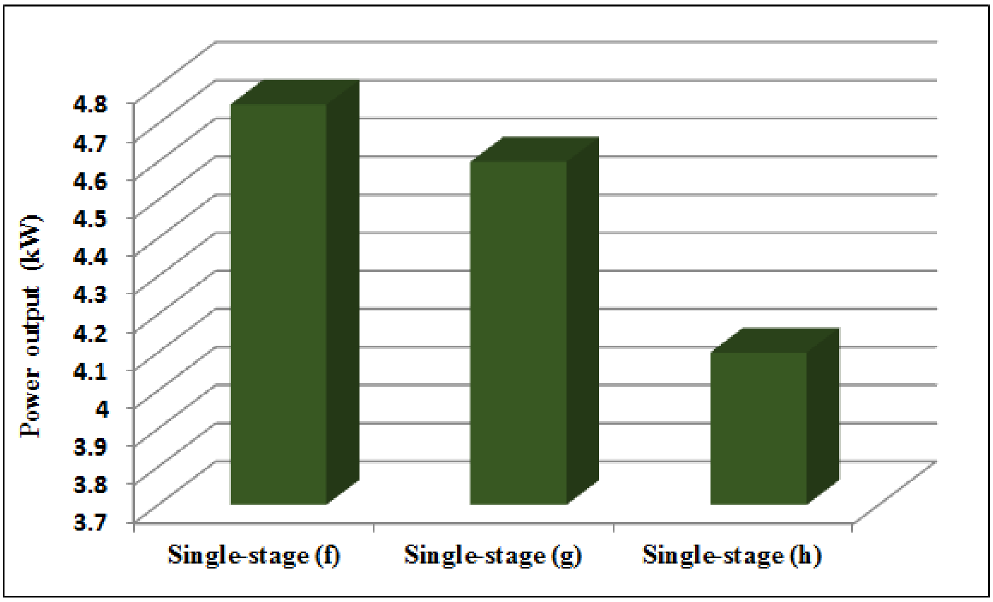

Fig. 14. Comparison of the power out put for various single-stage: single-stage (f) (r=48, e=6.6, b=32) mm, single-stage (g) (r=58, e=5, b=40) mm and single-stage (h) (r=48, e=6.6, b=64) mm.

Fig. 15 presents the power and isentropic efficiency with different rotating output speeds for the Wankel dimensions (r=48, e=6.6, b=32) mm and at (4 & 6) bar and 400 K, showing that increasing the rotational speed leads to increasing the power and an isentropic efficiency.

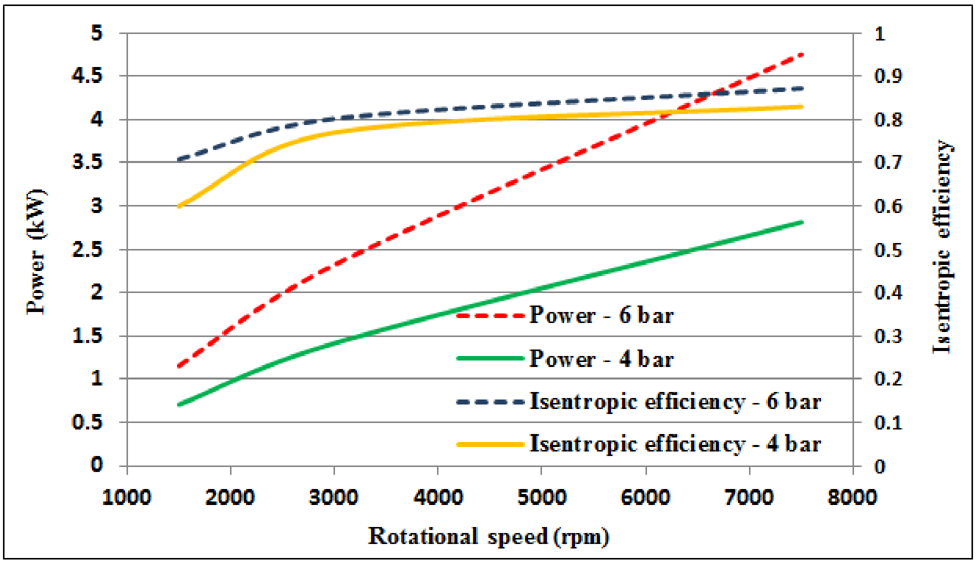

Fig. 15. Power output and Wankel expander isentropic efficiency for different rotating speeds

The performance of this Wankel expander was also evaluated at different inlet temperatures (350, 400, 450) K, inlet pressures (6 and 4) bar and 7500 rpm shaft speed. The maximimum isentropic efficiency reached (88 %) at 350 K and 6 bar with power output 4.6 kW as illustrated in Fig. 16.

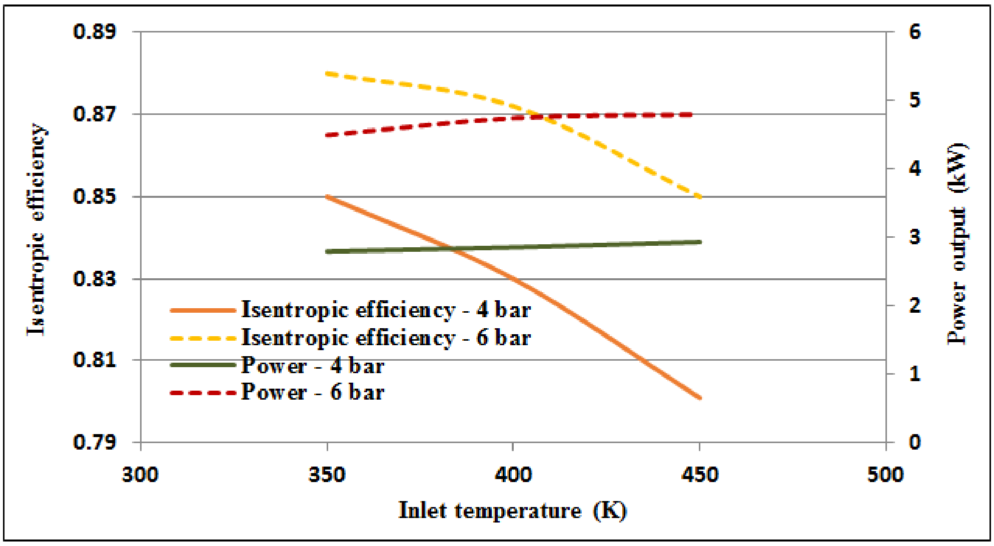

Fig. 16. Power output and Wankel expander isentropic efficiency for different inlet temperature

5. TWO-STAGEWANKLE EXPANDER

A number of two-stage Wankel expander configurations were investigated to achieve the highest power output as shown in table 3. In this table, three sizes of single-stage Wankel expander and five different two-stage configurations are described as shown in Fig. 17. In all two-stage expander configurations, the exit ports from the first stage are linked to the inlet ports of the second stage.

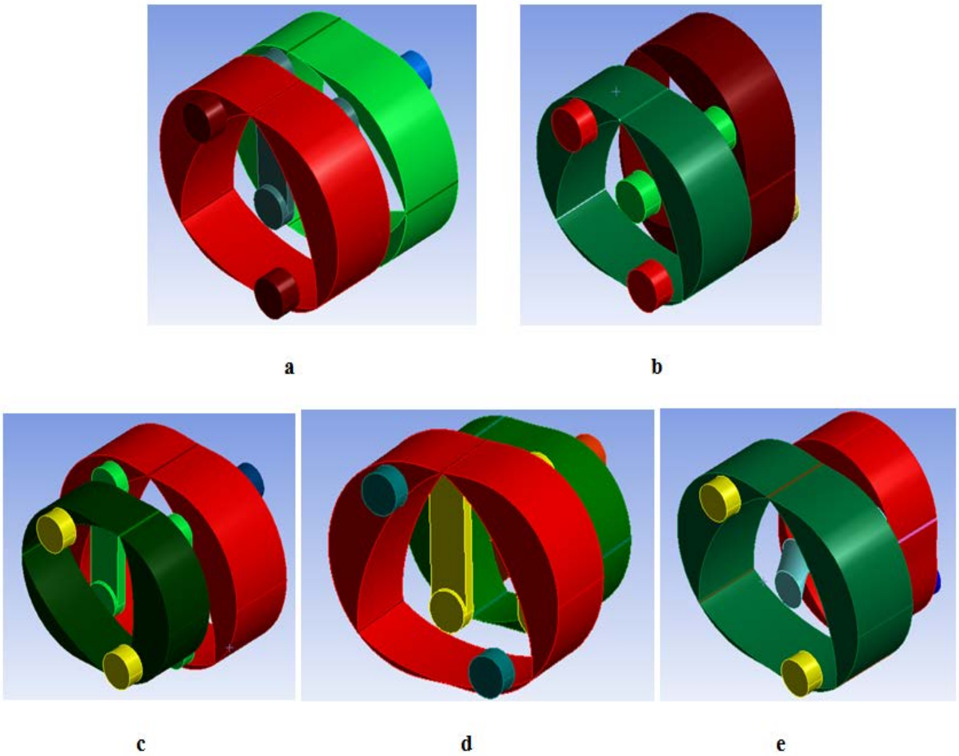

Fig. 17. Configurations of various two-stageWankel expanders (a) both horizontal – same size (b) 1st horizontal – 2nd vertical – same size (c) both horizontal – first smaller (d) both horizontal – second smaller (e) 1st horizontal - 2nd vertical – second smaller.

TABLE 3 TWO-STAGE EXPANDERS CONFIGURATIONS

No.	Details about the cases
1	**(a)** Two horizontal stages - same size (r=48, e=6.6, b=32) mm.
2	**(b)** Stage-stages - same size (r=48, e=6.6, b=32) mm, first stage horizontal and second stage vertical.
3	Two horizontal stages - different size **(c)** 1st stage (r=58, e=8, b=40) mm, 2nd stage (r=48, e=6.6, b=32) mm. **(d)** 1st stage (r=48, e=6.6, b=32) mm, 2nd stage (r=58, e=8, b=40) mm.
4	**(e)** Stage-stages - different size 1st stage horizontal (r=58, e=8, b=40) mm, 2nd stage vertical- (r=48, e=6.6, b=32) mm.
5	Single-stage **(f)** (r=48, e=6.6, b=32) mm, **(g)** (r=58, e=5, b=40) mm.

Fig. 18 compares the power output of the various two-stage configurations (a, b, c, d, and e) shown in Fig. 15 and the single-stage (f) with the dimensions (r = 48, e = 6.6, b = 32) mm at inlet pressure of 6 bar, inlet temperature 400 K and 7500 rpm. It can be seen that the Wankel expander with two horizontal stages (second stage smaller - d) produced the highest power output of 8.52kW.

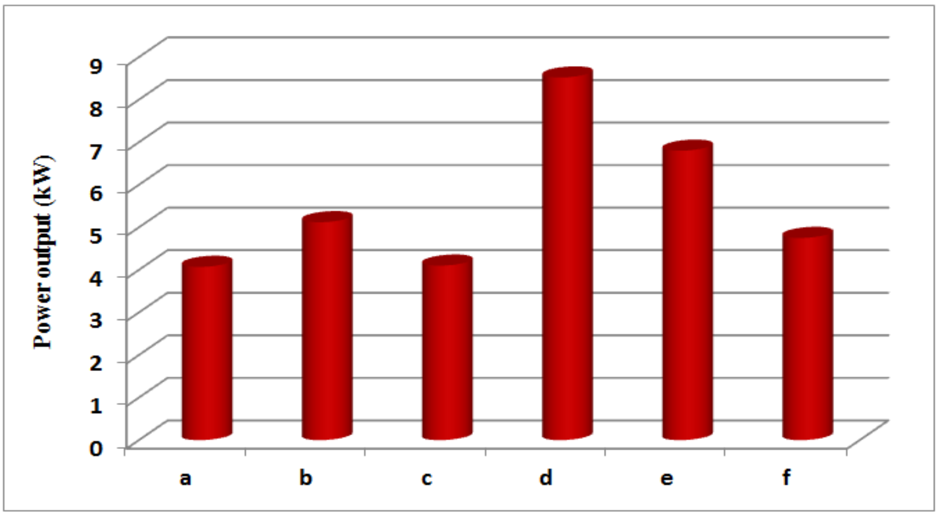

Fig. 18. Comparison between different two-stageWankel expander power output (a, b, c, d, and e) shown in Fig. 15 and the single-stage (f).

Fig. 19 presents the variation of the isentropic efficiency with different inlet pressures (4, 6, 8 & 12) bar, inlet temperature 400 K and 7500 rpm for the two horizontal stages, second stage smaller – d showing that a maximum isentropic efficiency of 91% at 6 bar.

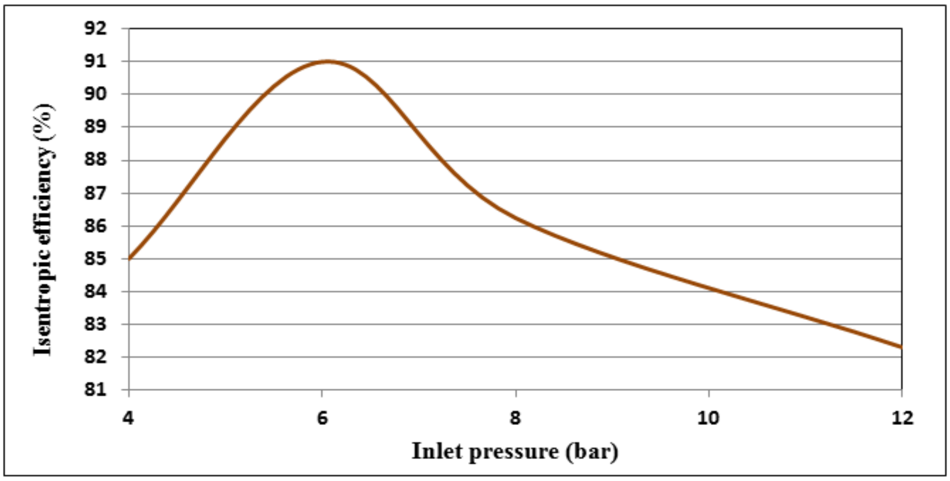

Fig. 19. Variation of the isentropic efficiency with different inlet pressure at 400 K and 7500 rpm

The comparison of the power output for the best two-stage Wankel expander configuration (d) with the single-stage (f) is shown in Fig. 20. It is clear from this figure that increasing the inlet pressure will increase the power output for both configurations, but the two-stage continuously outperforms the single-stage. Also, as the inlet pressure increases, the difference between the two-stage and single-stage power output increases, showing that the two-stage benefits more from increasing higher inlet pressure.

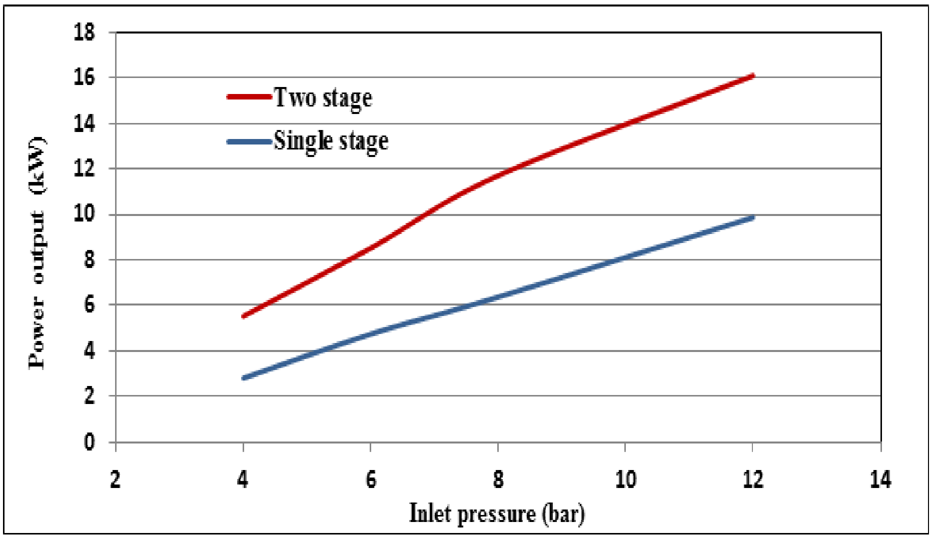

Fig. 20. Comparison between two-stage (d) and single-stage (f)

6. CONCLUSIONS

CFD ANSYS Fluent was successfully used to simulate the operation of the Wankel geometry as a single-stage and to develop a two-stageexpander device. The use of different parameters was investigated including the port configurations, location and size on the power output.

CFD results showed that circular port shape provides better performance than other shapes in terms of the power output and isentropic efficiency. Increasing the spacing between the ports leads to the power output increasing to reach a maximum of 4.75 kW at spacing of 50 mm and port diameter of 20 mm. Also the two horizontal stages – with first stage larger (r=58, e=8, b=40) mm than the second stage (r=48, e=6.6, b=32) mm, gave the highest power output of 8.52kW and isentropic efficiency of 91% at inlet pressure of 6 bar, inlet temperature of 400K and 7500 rpm. Increasing the inlet pressure will increase the power output for both single and two-stageconfigurations, but the two-stageone outperforms that of the single-stage at all inlet pressure values. Also, as the inlet pressure increases, the two-stagepower output improvement increases compared to that of the single-stage. This work highlights the potential of Wankel expanders in energy conversion.

Acknowledgement
The main author (Ghada Sadiq) gratefully acknowledges the Iraqi ministry of higher education and scientific research for funding the PhD scholarship at university of Birmingham, UK to develop the rotary Wankel engine for hybrid automotive application.

REFRENCE

[1] Norbye J. P, “TheWankel engine design development application.”, Published in Radnor, Pa., by Chilton Book Company and simultaneously in Ontrario, Canada, by Thomas Nelson & Sons, Ltd, third printing, February 1975.

[2] Ansdale R. F., “The Wankel RC Engine - Design and Performance.”, Published by ILIFFE, Books Ltd, London, UK, 1970.

[3] Yamamoto K., “Rotary Engines.” Published by Toyo Kogyo Co, Ltd, 1971.

[4] Spreitzer J., Zahradnik F., and B. Geringer, “Implementation of a Rotary Engine (Wankel Engine) in a CFD Simulation Tool with Special Emphasis on Combustion and Flow Phenomena,” SAE Tech. Pap., vol. 2015-April, no. April, 2015.

[5] Yamada T., Moriyoshi Y., “Numerical Analysis of Combustion and Flow Inside a Small Rotary Engine for Developing an Unmanned Helicopter,” *Assessment*, vol. 20076598, pp. 1–6, 2007.

[6] Jeng D.-Z., Hsieh M.-J., Lee C.-C., and Han Y., “The Numerical Investigation on the Performance of Rotary Engine with Leakage, Different Fuels and Recess sizes,” *SAE Tech. Pap.*, vol. 2013, 2013.

[7] Izweik H. T., “Cfd Investigations of Mixture Formation , Flow and Combustion for Multi-Fuel Rotary,” *Direct*, 2009.

[8] Amrouche F., Erickson P., Park J., and Varnhagen S., “An experimental investigation of hydrogen-enriched gasoline in a Wankel rotary engine,” *Int. J. Hydrogen Energy*, vol. 39, no. 16, pp. 8525–8534, 2014.

[9] Amrouche F., Erickson P. A., Varnhagen S., and Park J. W., “An experimental study of a hydrogen-enriched ethanol fueled Wankel rotary engine at ultra lean and full load conditions,” *Energy Convers. Manag.*, vol. 123, pp. 174–184, 2016.

[10] Warren S. and Yang D. C. H., “Design of rotary engines from the apex seal profile (Abbr.: Rotary engine design by apex seal),” *Mech. Mach. Theory*, vol. 64, pp. 200–209, 2013.

[11] Rose S. W. and Yang D. C. H., “Wide and multiple apex seals for the rotary engine: (Abbr.: Multi-Apex-Seals for the Rotary Engine),” *Mech. Mach. Theory*, vol. 74, pp. 202–215, 2014.

[12] Fan B., Pan J., Tang A., Pan Z., Zhu Y., and Xue H., “Experimental and numerical investigation of the fluid flow in a side-ported rotary engine,” *Energy Convers. Manag.*, vol. 95, pp. 385–397, 2015.

[13] Wang W., Zuo Z., and Liu J., “Miniaturization limitations of rotary internal combustion engines,” *Energy Convers. Manag.*, vol. 112, pp. 101–114, 2016.

[14] Yang L. J. and Wang T. H., “Design of a small Wankel engine,” *2012 7th IEEE Int. Conf. Nano/Micro Eng. Mol. Syst. NEMS 2012*, pp. 243–246, 2012.

[15] Ribau J., Silva C., Brito F. P., and Martins J., “Analysis of four-stroke, Wankel, and microturbine based range extenders for electric vehicles,” *Energy Convers. Manag.*, vol. 58, pp. 120–133, 2012

[16] Butti A. and V. Delle Site, “Wankel Engine for Hybrid Powertrain,” *SAE Tech. Pap.*, 1995.

[17] Varnhagen S., Same A., Remillard J., and Park J. W., “A numerical investigation on the efficiency of range extending systems using Advanced Vehicle Simulator,” *J. Power Sources*, vol. 196, no. 6, pp. 3360–3370, 2011.

[18] Heppner J. D., Walther D. C., and Pisano A. P., “The design of ARCTIC: A rotary compressor thermally insulated μcooler,” Sensors Actuators, A Phys., vol. 134, no. 1, pp. 47–56, 2007.

[19] Zhang Y. and Wang W., “Effects of leakage and friction on the miniaturization of a Wankel compressor,” *Front. Energy Power Eng. China*, vol. 5, no. 1, pp. 83–92, 2011.

[20] Yuqiao Z., Lam L. W., and Thong-see L., “CFD Simulation Of A Pump With Wankel Engine Geometry,” vol. 2001, no. 10, pp. 1–11, 2011.

[21] Badr O., Naik S., O’Callaghan P. W., and Probert S. D., “Wankel engines as steam expanders: Design considerations,” *Appl. Energy*, vol. 40, no. 3, pp. 157–170, 1991.

[22] Badr O., Naik S., O’Callaghan, and Probert S. D., “Expansion machine for a low power-output steam Rankine-cycle engine,” *Appl. Energy*, vol. 39, no. 2, pp. 93–116, 1991.

[23] Badr O., Naik S., O’Callaghan P. W., and Probert S. D., “Rotary Wankel engines as expansion devices in steam Rankine-cycle engines,” Appl. Energy, vol. 39, no. 1, pp. 59–76, 1991.

[24] M. Antonelli, A. Baccioli, M. Francesconi, U. Desideri, and L. Martorano, “Operating maps of a rotary engine used as an expander for micro-generation with various working fluids,” Appl. Energy, vol. 113, pp. 742–750, 2014.

[25] Antonelli M., Baccioli A., Francesconi M., and Martorano L., “Experimental and numerical analysis of the valve timing effects on the performances of a small volumetric rotary expansion device,” Energy Procedia, vol. 45, pp. 1077–1086, 2014.

[26] Antonelli M., A. Baccioli, Francesconi M., R. Lensi, and L. Martorano, “Analysis of a low concentration solar plant with compound parabolic collectors and a rotary expander for electricity generation,” *Energy Procedia*, vol. 45, pp. 170–179, 2014.

[27] Antonelli M. and Martorano L., “A study on the rotary steam engine for distributed generation in small size power plants,” *Appl. Energy*, vol. 97, pp. 642–647, 2012.

[28] Rosario J. D., “Fabrication and assembly of a 2.4 mm compressed gas rotary expander,” M.Sc. Dissertations, University of California, Berkeley, 2005.

[29] Yamamoto K., “Rotary engine,” Published by Sankaido Co. Ltd, Tokyo, Japan, 1981.

[30] ANSYS FLUENT, User’s Guide (Release 16.2). ANSYS, Inc., 2015.

[31] Solidworks. (2015). Dassault Systèmes

[32] Excel. (2010). Microsoft.

[33] ANSYS FLUENT, Theory Guide (Release 16.2). ANSYS, Inc., 2015.

[34] MATLAB (2013), Math works.